Molecular Mechanism of Solvent-Induced Crystallization of Syndiotactic Polystyrene Glass. 1. Time-Resolved Measurements of Infrared/Raman Spectra and X-ray Diffraction

Kohji Tashiro,* Yoko Ueno, Akiko Yoshioka, and Masamichi Kobayashi

Department of Macromolecular Science, Graduate School of Science, Osaka University, Toyonaka, Osaka 560-0043, Japan

Received September 26, 2000; Revised Manuscript Received October 26, 2000

ABSTRACT: Time-resolved measurements of FT-IR and Raman spectra and X-ray diffraction have been performed to trace the structural changes in the solvent-induced crystallization of syndiotactic polystyrene glass sample. After the exposure of the glassy sample into the atmosphere of such organic solvent as toluene, benzene, or chloroform, the IR and Raman bands characteristic of the regular helical conformation of $(T_2G_2)_2$ type were found to increase the intensities with time. Some time delay was found for the appearance of the bands with different critical sequence lengths, leading to the concrete description of the growth of regular helical chain from the random coil. The X-ray scattering intensity began to increase largely at the timing of the appearance of the IR and Raman bands of long helical sequences, indicating that the crystal lattice starts to be formed at the timing when the long segments of regular helical form are gathered together. The rate of this crystallization process depends on the kind of the used solvent. The factors governing this difference have been discussed.

Introduction

Syndiotactic polystyrene (*s*PS) is one important species of the polystyrene family including atactic (*a*PS) and isotactic (*i*PS) polystyrene. *s*PS has two types of molecular chain conformations in its crystalline region,[1−26] as shown in Figure 1. Roughly speaking, random coils of the glassy state regularize to the planar zigzag form in the α and β crystalline forms by annealing the glass sample above the glass transition temperature and to a complex of $(T_2G_2)_2$ form with solvent by absorption of organic solvents (δ form). By heating the δ form above 130 °C, it is transformed to the γ form with keeping the chain conformations of $(T_2G_2)_2$ form. This γ form transfers to the planar zigzag form (α and β forms) by heat treatment at higher temperature. In this way *s*PS shows a very complicated polymorphism. These changes remarkably depend on such various conditions as the thermal history of the samples, the kind of solvent, etc. The crystal structures of these modifications were analyzed by many researchers, but the evolution mechanism of the structural change in these phase transition phenomena has not yet been understood enough clearly.

In the present paper, we focus our attention on the solvent-induced crystallization process of the *s*PS glass. Although several papers were published so far about the formation of complex between polymer and solvent,[27−29] the microscopically viewed crystal formation process was quite limited, and the details have not yet been clarified at all. For this purpose we combined the various types of apparatuses such as FT-IR, Raman, and wide-angle X-ray scattering (WAXS) and carried out the time-resolved measurements during the solvent-induced crystallization phenomenon. On the basis of these experimental data, the concrete structural evolution will be described from the viewpoints of molecular chain conformation and the crystal lattice.

Experimental Section

Samples. The *s*PS powder (M_w 272 000, M_w/M_n 2.28) was kindly supplied by Idemitsu Petrochemical Co., Ltd. The glassy samples were prepared by quenching the molten *s*PS films into liquid nitrogen. A check of the amorphous content was made by measuring the FT-IR and X-ray diffraction pattern at room temperature. The thickness of the samples used for the time-resolved IR measurements was 50 μm and about 100 μm for Raman and WAXS measurements.

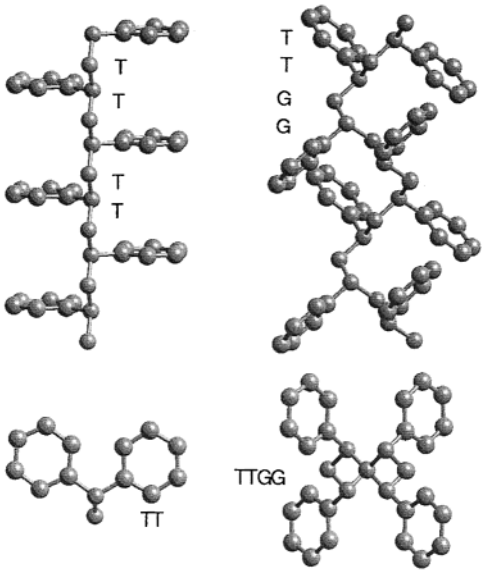

Figure 1. Molecular chain conformations of the crystalline phases of *s*PS.

Measurements. In the time-resolved measurements of X-ray diffraction and IR and Raman spectra for the samples subjected to the solvent atmosphere, the homemade cells were used as shown in Figure 2. The measurement was started at the same time with the solvent injection, and the data were saved at a constant time interval. In these experiments the solvent vapor might be assumed in a good approximation to fill the small sample cell quite rapidly after the solvent injection. Therefore, the solvent injection time was set equal to the starting time of the measurements. The infrared spectra were taken at a resolution power 2 cm^{-1} at a time interval of 16 s by using a Bio-Rad FTS-60A FT-IR spectrometer equipped

10.1021/ma001659s CCC: $20.00
Published on Web 12/14/2000

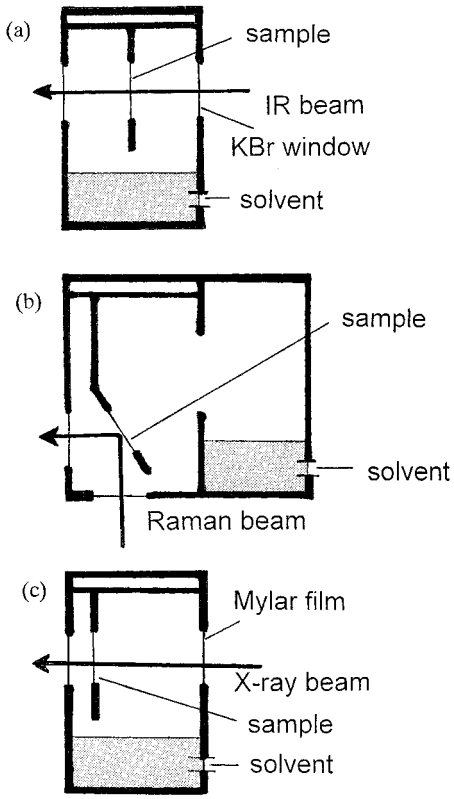

Figure 2. Sample cells used for the time-resolved measurements for the samples subjected to the solvent atmosphere: (a) for IR, (b) for Raman, and (c) for X-ray scattering.

with an MCT detector. The WAXS patterns were obtained at a time interval of 1 min with graphite-monochromatized Cu Kα radiation (40 kV and 200 mA) by using DIP1000 of MAC Science Co., Ltd. The CCD detector (C 4880-20, Hamamatsu Photonics Co., Ltd., Japan) was used, and the reflection profile was calculated by integrating the 2-D pattern over a proper angle range. The Raman spectra were taken by a JASCO (Japan Spectroscopic Co., Ltd.) NR1800 Raman spectrometer equipped with a 514.5 nm Ar^+ ion laser as an excitation light source. The 90° scattering light was collected at 2 cm^{-1} resolution at a time interval of 90 s. All the spectral profiles obtained by the above-mentioned experiments were separated into components by a deconvolution technique in order to make the quantitative analyses as will be mentioned in later sections. The used solvents were chloroform, benzene, and toluene.

Results and Discussion

Formation Process of Helical Chains. Parts a, b, and c of Figure 3 show the IR spectral changes of *s*PS glass samples exposed to a solvent atmosphere, where chloroform, benzene, and toluene were used as the solvent, respectively. The bands characteristic of the solvent and the T_2G_2 conformation[1,4,9,12,19] were observed to increase their intensities, and the amorphous bands decreased the intensities with a passage of time after solvent injection. Deconvolution of the overlapped bands was made in the frequency region of 600−450 cm^{-1}. Figures 4 and 5 show the time dependencies of the integrated intensities of these bands estimated for the two cases of toluene and benzene solvents, respectively. The solvent band started to increase the intensity soon after the injection into the sample cell. From this curve the diffusion coefficient of the solvent molecule might be evaluated, but this evaluation was not made here

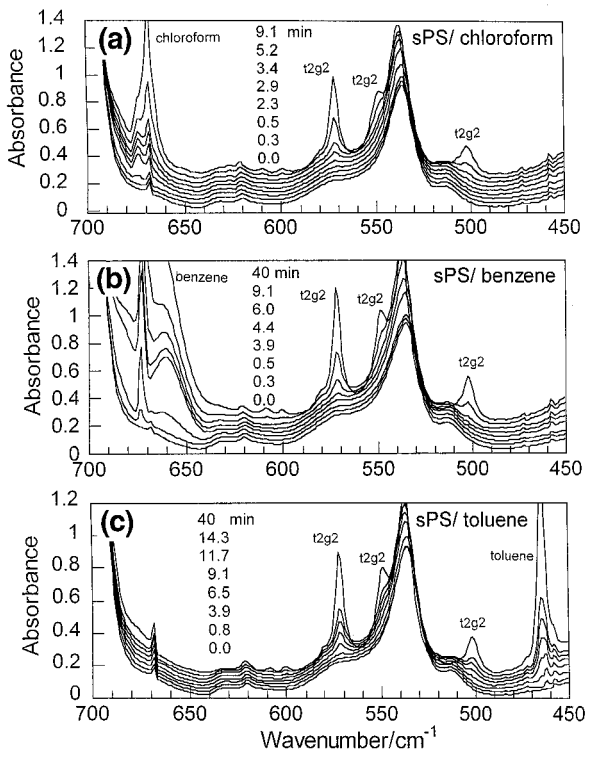

Figure 3. Time dependence of the infrared spectra of *s*PS glass sample exposed to solvent atmosphere at room temperature: (a) chloroform, (b) benzene, and (c) toluene.

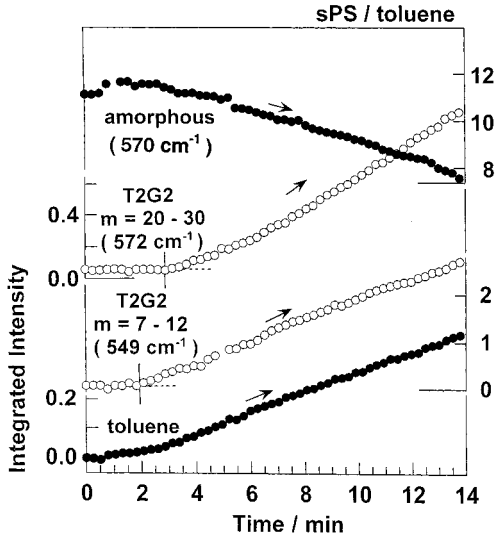

Figure 4. Time dependence of the integrated intensities of the infrared bands estimated for the *s*PS glass exposed to toluene atmosphere.

because the solvent molecules were considered to behave in a complicated manner, including the diffusion, the adsorption, and the formation of complex with polymer chains. It should be noticed in Figures 4 and 5 that the timing of detection of the band intensity is different between the bands, although they are commonly the bands characteristic of the T_2G_2 conformation. For example, as shown in Figure 4, the band at 549 cm^{-1} begins to be observed around 2 min later after the appearance of the toluene band. The band at 572 cm^{-1} could be detected about 3 min later. Figure 6 shows the Raman spectral changes of the *s*PS glass sample exposed to a toluene atmosphere. Similar to the case of

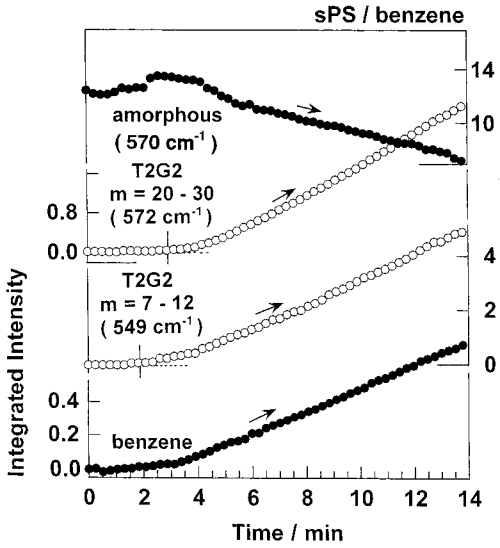

Figure 5. Time dependence of the integrated intensities of the infrared bands estimated for the *s*PS glass exposed to benzene atmosphere.

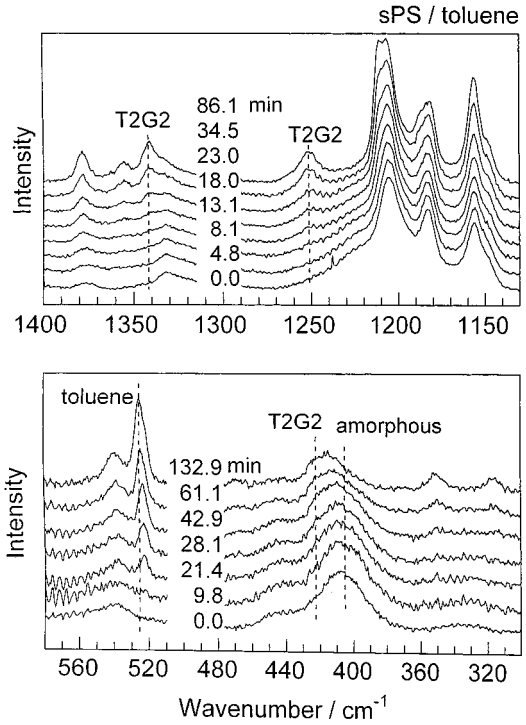

Figure 6. Time dependence of the Raman spectra measured for *s*PS glass sample exposed to toluene atmosphere at room temperature.

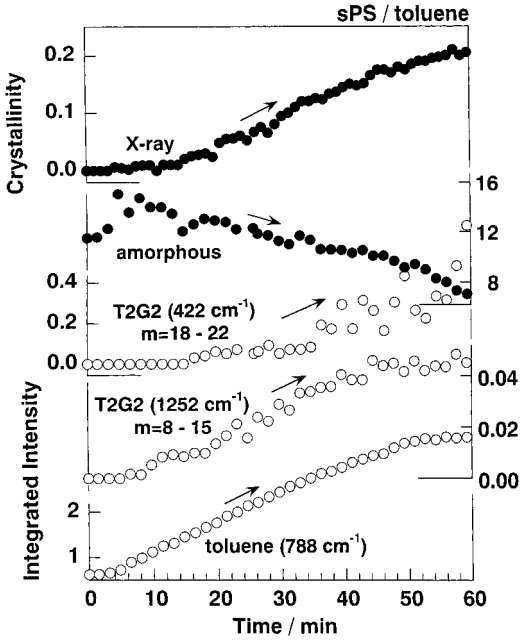

Figure 7. Time dependence of the integrated intensities of the Raman bands estimated for the *s*PS glass exposed to toluene atmosphere. The X-ray scattering intensity evaluated from the data of Figure 10 is also plotted.

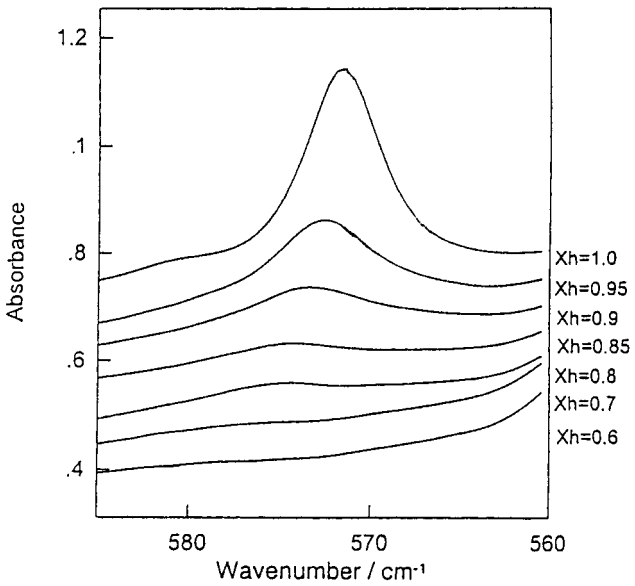

Figure 8. Infrared spectra measured for a series of *s*PS copolymers with various H/D contents, where the samples were of the δ form. X_h is the molar fraction of the H component in the copolymer.

the IR spectral change, the bands characteristic of toluene and T_2G_2 form increased the intensities with time while the amorphous bands decreased in intensity. In this case of Raman spectra also, the timing of the appearance was different among the bands (Figure 7). These phenomena could be observed for all the cases of toluene, benzene, and chloroform.

Kobayashi et al. proposed the concept of critical sequence length *m* as a measure of the different sensitivity of the various bands.[30] By utilizing this concept, the concrete reason may be deduced for the above-mentioned difference in the timing of the appearance of the different bands, from which the structural evolution in the amorphous state may be described. The critical sequence length *m* could be evaluated by the method reported by Kobayashi et al.[30] In this evaluation a series of random copolymers between the hydrogeneous and deuterated styrene monomers were synthesized and were used for the infrared and Raman measurements. One example of the infrared spectra of these samples taken at room temperature is given in Figure 8. The intensity of the band of the H species at 572 cm^{-1} decreased systematically with a decrement of the H content in the copolymers. Figure 9 shows the relation between the reduced intensity $R(X)/R(1.0)$ and the molar fraction of the H species X, where $R(1.0)$ is the integrated intensity of the pure H polymer. On the basis of the Markov statistics, the $R(X)/R(1.0)$ is ex-

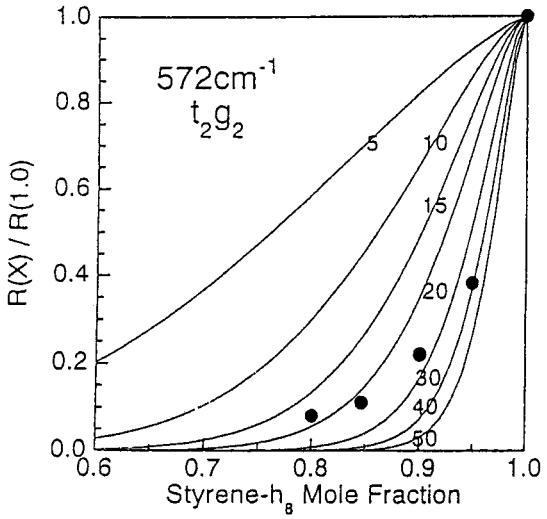

Figure 9. A plot of the reduced intensity of the 572 cm^{-1} infrared band against the molar fraction of the H component of *s*PS copolymer. The data are compared with the theoretical curves calculated for the various critical sequence length *m*.

pressed by the following equation:

$$R(X)/R(1.0) = X^m[1 + (m - 1)X] \qquad (1)$$

By comparing the observed data with the theoretical curve predicted by eq 1, the critical sequence length *m* can be determined. For the 572 cm^{-1} band, *m* is 20−30. The similar process was made for many bands of both the IR and Raman spectra. The thus determined *m* values are listed in Table 1. The details will be reported elsewhere.

At this stage Figures 4 and 5 are seen again. The 549 cm^{-1} band with $m = 7-12$ monomeric units is found to increase the intensity after the growth of solvent band. The band at 572 cm^{-1} with larger *m* values of 20−30 increases the intensity with further longer delay. Therefore, it may be said that the short helical segments consisting of 7−12 monomeric units are formed with some induction period after the injection of the solvent. Since the bands with large *m* values take longer time to be observed in the spectra, it can be said that these short helices grow to longer helices with passage of time. This is a quite natural description about the growth of regular helical chain segment but could be experimentally proved for the first time by carrying out the time-resolved measurements of the vibrational spectra.

As one of the important questions concerning the solvent-induced crystallization, we need to clarify the question whether the crystallization phenomenon is limited by solvent diffusion or not. In association with this question, it may be important to clarify the relation between the solvent diffusion behavior and the helix formation process of the polymer chains. But, because the quantitative analysis of the diffusion behavior of the solvent was difficult at the present stage, this significant question is still unsettled as a future work.

Figure 10 shows the result of the time-resolved X-ray scattering measurement by using the CCD camera system. With the passage of time, the reflection peaks originated from the crystalline region could be detected relatively clearly. As for the X-ray reflection profiles shown in this figure, we may notice that the profile is not as sharp as that observed usually for the sample

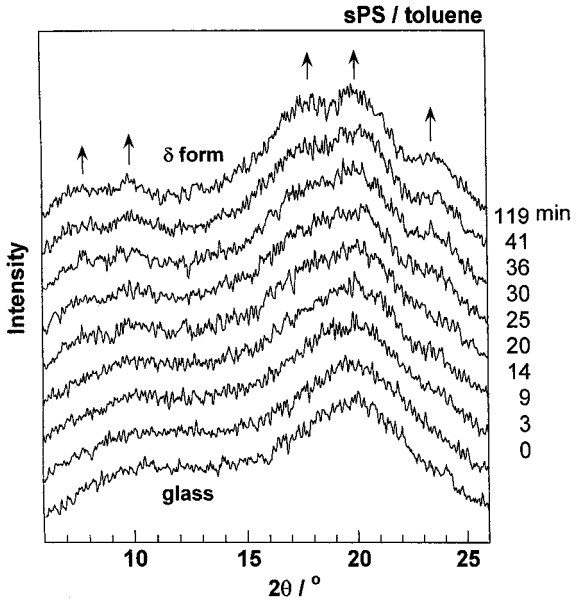

Figure 10. Time dependence of the X-ray scattering profile measured for the *s*PS glass sample exposed to toluene atmosphere at room temperature.

Table 1. Critical Sequence Lengths *m* Evaluated for the Various IR/Raman Bands of All-Trans and T_2G_2 Conformations of *s*PS Crystalline Forms

all-trans conformation		*m*
infrared band	1222 cm^{-1}	30−50
	1333 cm^{-1}	10−15
	1375 cm^{-1}	20−30
Raman band	230 cm^{-1}	2−5
	526 cm^{-1}	10−15
	773 cm^{-1}	10−12
	857 cm^{-1}	>50
	1320 cm^{-1}	5−10
T_2G_2 conformation		*m*
infrared band	502 cm^{-1}	12−20
	549 cm^{-1}	7−12
	572 cm^{-1}	20−30
	1168 cm^{-1}	20−30
	1277 cm^{-1}	12−15
	1353 cm^{-1}	12−15
Raman band	243 cm^{-1}	2−5
	422 cm^{-1}	18−22
	536 cm^{-1}	5−10
	802 cm^{-1}	8−16
	1252 cm^{-1}	8−12

once dipped to the solvent and dried up at room temperature. This can be said even after the long time passed in the present experiment. The reason may come from the effect of newly coming solvent which dissolves the parts of crystalline regions more or less after the crystallization, because the solvent works as a good solvent for *s*PS. The case of chloroform was more remarkable, though the data are not given here. From Figure 10, the intensity of the crystalline peaks was evaluated and was plotted against time in comparison with the Raman spectral data as shown in Figure 7. In this experiment the sample thickness and the experimental conditions were essentially the same with those of the Raman experiment shown in Figures 6 and 7, allowing us a comparison between the Raman and X-ray diffraction data. The X-ray scattering from the crystalline region starts to be detected in the time region where the Raman bands with long critical sequence length *m* of 18−22 monomeric units start to increase their

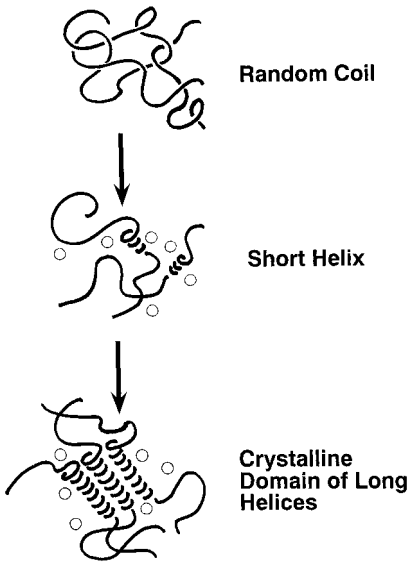

Figure 11. An illustration of the structural evolution in the process of solvent-induced crystallization of *s*PS glass.

intensities. It may be considered that the short helical segments grow to longer helices and gather together to form an aggregation structure which can be detected as the X-ray scattering from the crystal lattice. The concrete illustration of this structural change is shown in Figure 11. It must be emphasized again that the structural evolution shown in this figure is quite natural but could be found for the first time by carrying out the combination of the various kinds of measurements. Another important point is that the X-ray data told us the formation of the crystal lattice in the time region where the long helical segments are developed from the short helices. But, even at the initial stage of formation of such short helical segments, they might form the domains of some finite size which cannot be detected by the present X-ray measurements. These domains are speculated to play a role as a nucleus for the formation of the crystallite of longer size.

Solvent Effect: Crystallization and Gelation. It may be naturally expected that the crystallization behavior is affected more or less by the type of the used organic solvent. We measured the time dependence of the FT-IR spectra for the organic solvents of chloroform, benzene, and toluene and compared the crystallization rate among them. To carry out this comparison quantitatively, the film thickness was adjusted to almost the same value. Figure 12 shows the time evolution of the crystalline fraction evaluated from the IR spectra. The T_2G_2 bands begin to appear after the observation of some induction time, which depends remarkably on the kind of the used solvent. The slope of the curve, i.e., the crystallization rate, is also different. The induction period and the crystallization rate are changed in the order of $CHCl_3 \gg C_6H_6 \geq C_6H_5CH_3$.

Kobayashi et al. evaluated the gelation rate of *s*PS dilute solution by the time-resolved FT-IR measurement for such various kinds of solvent as benzene, chloroform, and carbon tetrachloride.[31−34] The chloroform causes quite slow gelation compared with benzene or carbon tetrachloride. This difference in the gelation rate between chloroform and benzene is quite in contrast to the difference in the solvent-induced crystallization rate as mentioned above. As a result, we have the following

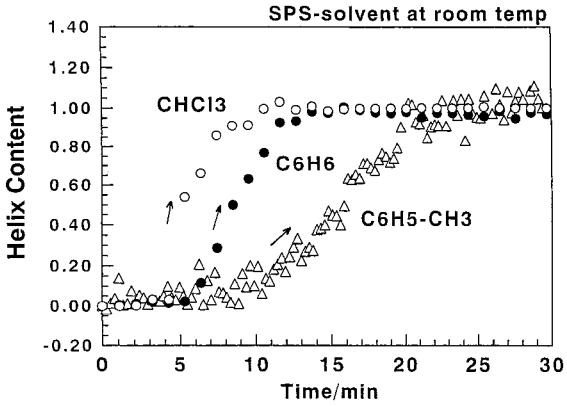

Figure 12. Comparison of the time dependence of the infrared intensity of the crystalline bands estimated for the *s*PS glass samples subjected to the various kinds of solvent atmosphere (room temperature).

relation:

gelation: $CHCl_3 \ll C_6H_6$

crystallization: $CHCl_3 \gg C_6H_6 \geq C_6H_5CH_3$

Why is such a quite contrast tendency observed between the gelation and crystallization phenomena? It may be possible to interpret this difference qualitatively in terms of (i) the easiness of invasion and migration of the solvent molecules into the *s*PS sample, (ii) the stabilization energy in the formation of the *s*PS−solvent complex, and so on.[35−39] Factor (i) is associated with the bulkiness of the solvent molecule and the solubility of *s*PS in the solvent or the interaction between the solvent and *s*PS. As already mentioned,[40] the solvent induces the molecular motion of the amorphous polymer chains, indicating that the solvent dissolves the polymer chains even partly in the glassy state and plays as a kind of plasticizer. This activated chain motion causes the generation of the crystalline nuclei. Therefore, the solvent giving higher solubility of *s*PS is considered to give the higher nucleation rate and higher crystallization rate. The solvent molecules are needed, of course, to invade into the polymer sample prior to the diffusion in the sample. This motion is related also with the bulkiness of the molecule: the smaller molecule is easier to penetrate into the sample and pass through the voids of the polymer network. Factor (ii) is the thermodynamic effect: the complex formation is accelerated if the *s*PS−solvent complex system is energetically stabilized. The gelation, on the other hand, causes the formation of cross-linkages which are considered to be essentially equivalent to the crystalline state of the *s*PS−solvent complex. In the dilute solution the random coils are dipped in the sea of solvent and are surrounded by many solvent molecules. But, to form the cross-linkages or the stoichiometric polymer−solvent complex, the surplus solvent molecules must be purged out of the random coils. That is to say, the solvent with lower solubility tends to give more easily the cross-linkage parts. In other words, the solvent system with the higher solubility may give the slower gelation process.

In this way the difference in the solubility and bulkiness of solvents can allow us to interpret qualitatively the difference in the complex formation rate between the gelation and the crystallization. At room temperature the *s*PS is quite easily dissolved in chloroform than in benzene. Therefore, we may expect the

following tendency, which corresponds well to the actually observed results.

solubility: $CHCl_3 > C_6H_6$

bulkiness: $CHCl_3 < C_6H_6$

crystallization: $CHCl_3 > C_6H_6$

gelation: $CHCl_3 < C_6H_6$

In other words, the interactions between *s*PS and organic solvent molecules seem to play a quite important role in the formation process of gel and crystal, although they work oppositely in these two transition phenomena.

Conclusions

In this paper we described the structural evolution in the solvent-induced crystallization process of the glassy *s*PS. The time-resolved measurements were made successfully for the infrared, Raman, and X-ray diffraction, from whose data the details of the structural regularization process could be clarified for the first time from the points of molecular conformation as well as the chain aggregation structure. The rate of this ordering process was found to be dependent on the kind of the used solvent. By comparing with the case of gelation from the solution, several key factors governing these ordering processes (crystallization and gelation) were extracted.

The reader may notice here that this solvent-induced crystallization process occurs at room temperature. The glass transition temperature of *s*PS is above 100 °C. Therefore, it might be difficult to speculate the reasons why the crystallization occurs so fast even below the glass transition temperature where the chain motions are frozen. Of course, we might be able to say that this crystallization is caused by the solvent working as a plasticizer. But we must demonstrate concretely an occurrence of the chain motion induced by the solvent. This experimental proof of the chain motion in the amorphous region is quite important to understand the crystallization process of this polymer from the molecular level. The detailed results will be reported soon elsewhere.[40]

Acknowledgment. The authors thank the Idemitsu Petrochemical Co., Ltd., Japan, for supplying *s*PS samples. They also thank Mr. Mitsuo Ohama (Graduate School of Science, Osaka University) for his help in the time-resolved measurement of the Raman spectra.

References and Notes

(1) Kobayashi, M.; Nakaoki, T.; Ishihara, N. *Macromolecules* **1989**, *22*, 4377.
(2) Greis, O.; Xu, Y.; Petermann, J. *Polymer* **1989**, *30*, 590.
(3) Guerra, G.; Vincenzo, V.; Vitagliano, M.; De Rosa, C.; Petraccone, V.; Corradini, P. *Macromolecules* **1990**, *23*, 1539.
(4) Kobayashi, M.; Nakaoki, T.; Ishihara, N. *Macromolecules* **1990**, *23*, 78.
(5) Zimba, C. G.; Rabolt, J. F. *Macromolecules* **1989**, *22*, 2867.
(6) Reynolds, N. M.; Hsu, S. L. *Macromolecules* **1990**, *23*, 3463.
(7) De Rosa, C.; Guerra, G.; Petraccone, V.; Corradini, P. *Polym. J.* **1991**, *23*, 1435.
(8) Vittoria, V.; Russo, R.; de Candia, F. *Polymer* **1991**, *32*, 3371.
(9) Reynolds, N. M.; Stidham, H. D.; Hsu, S. L. *Macromolecules* **1991**, *24*, 3662.
(10) Kobayashi, M.; Nakaoki, T. *J. Mol. Struct.* **1991**, *242*, 315.
(11) Chatani, Y.; Shimane, Y.; Inoue, Y.; Inagaki, T.; Ijitsu, T.; Yukinari, T. *Polymer* **1992**, *33*, 488.
(12) De Rosa, C.; Rapacciuolo, M.; Guerra, G.; Petraccone, V.; Corradini, P. *Polymer* **1992**, *33*, 1423.
(13) Chatani, Y.; Shimane, Y.; Ijitsu, T.; Yukinari, T. *Polymer* **1993**, *34*, 1625.
(14) Chatani, Y.; Shimane, Y.; Inagaki, T.; Ijitsu, T.; Yukinari, T.; Shikuma, H. *Polymer* **1993**, *34*, 1620.
(15) Chatani, Y.; Inagaki, T.; Shimane, Y.; Shikuma, H. *Polymer* **1993**, *34*, 4841.
(16) Sun, Z.; Millar, R. L. *Polymer* **1993**, *34*, 1963.
(17) Corradini, P.; DeRosa, C.; Guerra, G.; Napolitano, R.; Petraccone, V.; Porozzi, B. *Eur. Polym. J.* **1994**, *30*, 1173.
(18) Vittoria, V.; Russo, R.; de Candia, F.; Carotenuto, M.; Guadagno, L. *J. Macromol. Sci., Phys.* **1996**, *B35*, 265.
(19) Kellar, E. J. C.; Galiotis, C.; Andrews, E. H. *Macromolecules* **1996**, *29*, 3315.
(20) De Rosa, C. *Macromolecules* **1996**, *29*, 8460.
(21) Kellar, E. J. C.; Evans, A. M.; Knowles, J.; Galiotis, C.; Andrews, E. H. *Macromolecules* **1997**, *30*, 2400.
(22) Tosaka, M.; Hamada, N.; Tsuji, M.; Kohjiya, S.; Ogawa, T.; Isoda, S.; Kobayashi, T. *Macromolecules* **1997**, *30*, 4132.
(23) Hamada, N.; Tosaka, M.; Tsuji, M.; Kohjiya, S.; Katayama, K. *Macromolecules* **1997**, *30*, 6888.
(24) Tosaka, M.; Hamada, N.; Tsuji, M.; Kohjiya, S. *Macromolecules* **1997**, *30*, 6592.
(25) De Rosa, C.; Guerra, G.; Petraccone, V.; Pirozzi, B. *Macromolecules* **1997**, *30*, 4147.
(26) Guerra, G.; Manfredi, C.; Musto, P.; Tavone, S. *Macromolecules* **1998**, *31*, 1329.
(27) Tsutsui, K.; Katsumata, T.; Fukatsu, H.; Yoshimizu, H.; Kinoshita, T.; Tsujita, Y. *Polym. J.* **1999**, *31*, 268.
(28) Tsutsui, K.; Katsumata, T.; Yamamoto, Y.; Fukatsu, H.; Yoshimizu, H.; Kinoshita, T.; Tsujita, Y. *Polymer* **1999**, *40*, 3815.
(29) Vittoria, V.; Filho, A. R.; de Candia, F. *Polym. Bull.* **1991**, *26*, 445.
(30) Kobayashi, M.; Akita, K.; Tadokoro, H. *Makromol. Chem.* **1968**, *118*, 324.
(31) Kobayashi, M.; Kozasa, T. *Appl. Spectrosc.* **1993**, *47*, 1417.
(32) Kobayashi, M.; Yoshioka, T.; Kozasa, T.; Suzuki, J.; Funahashi, S.; Izumi, Y. *Macromolecules* **1994**, *27*, 1349.
(33) Kobayashi, M.; Yoshioka, T.; Imai, M.; Itoh, Y. *Macromolecules* **1995**, *28*, 7376.
(34) Kobayashi, M. *Macromol. Symp.* **1997**, *114*, 1.
(35) Musto, P.; Manzari, M.; Guerra, G. *Macromolecules* **2000**, *33*, 143.
(36) Tashiro, K.; Ueno, Y.; Yoshioka, A.; Kaneko, F.; Kobayashi, M. *Macromol. Symp.* **1999**, *141*, 33.
(37) Daniel, C.; Menelle, A.; Brulet, A.; Guenet, J. M. *Macromol. Symp.* **1997**, *114*, 159.
(38) Guenet, J. M. *Macromol. Symp.* **1997**, *114*, 97.
(39) Daniel, C.; Menelle, A.; Brulet, A.; Guenet, J. M. *Polymer* **1997**, *38*, 4193.
(40) Tashiro, K.; Sasaki, S.; Ueno, Y.; Yoshioka, A.; Kobayashi, M. *Korea Polym. J.* **2000**, *8*, 103.

MA001659S